Design guidelines for transition metals as interstitial emitters in silicon nanocrystals to tune photoluminescence properties: Zinc as biocompatible example

– Electronic Supplemental Information –

Dirk König,*[a, b, 1] Richard D. Tilley,[b] and Sean C. Smith[c, a]

[a]Integrated Materials Design Lab (IMDL), The Australian National University, ACT 2601, Australia.
*E-mail: solidstatedirk@gmail.com
[b] School of Chemistry, University of New South Wales, Sydney, NSW 2052, Australia.
[c] Department of Applied Mathematics, Research School of Physics and Engineering, The Australian National University, ACT 2601, Australia.

1 Further data on and discussion of the exchange and correlation interactions

From the left graph in Figure 1 we see that the eigenenergies of the i-Zn fontier OMOs split proportional to $[d_{\mathrm{Zn}\cdots\mathrm{Zn}}]^{-1}$, *i.e.* proportional to the inverse distance between i-Zn dopants. At such short distances, this splitting can be clearly assigned to Pauli blocking [1, 2]. In addition, we see from the same graph that the increase of energy splitting is not symmetric. This asymmetry becomes most significant for 4× i-Zn dopants as a function of their distance, *i. e.* i-Zn near the NC surface *vs.* half-way into the NC. The right graph of Figure 1 presents the relevant data in a more convenient form, namely the evolution of the eigenenergy average of i-Zn frontier OMOs with the distance between and number of i-Zn dopants. We can clearly see the hyperbolic behaviour of the exchange interaction.

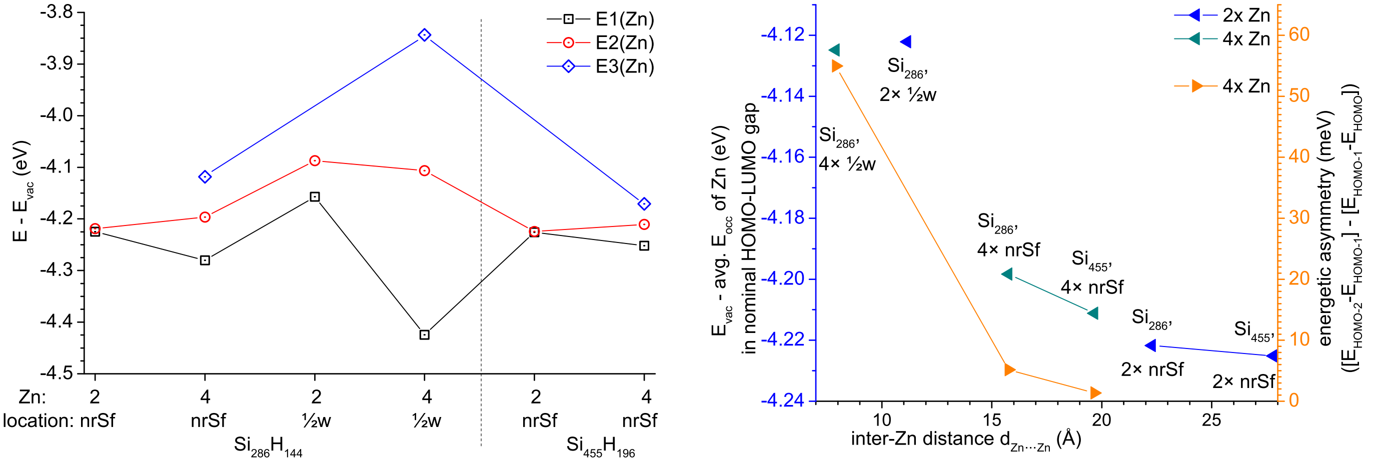

Figure 1: Eigenenergies of frontier OMOs due to i-Zn relative to vacuum level E_{vac} for all doped approximants (left), see also to Figs. 3 and 4 in main publication. Abscissa shows respective number and location of i-Zn dopants (near surface – nrSf, half-way into NC – $^1/_2$w), and the respective Si NC with $d_{\mathrm{NC}}(\mathrm{Si}_{286}) = 22$ Å, and $d_{\mathrm{NC}}(\mathrm{Si}_{455}) = 26$ Å, *cf.* Fig. 1 in main publication. Average energy of all of frontier OMOs due to i-Zn and asymmetry of level splitting as a function of i-Zn distance $d_{\mathrm{Zn}\cdots\mathrm{Zn}}$ (right).

The other parameter referring to the right y-axis accounts for the asymmetry in energy splitting by calculating $(E_3 - E_2) - (E_2 - E_1)$, being zero for full symmetry ($[E_3 - E_2] = [E_2 - E_1]$). This asymmetry is caused by a

---

[1] Also at the Institute of Semiconductor Electronics (IHT), RWTH Aachen University, 52074 Aachen, Germany

change in correlation interaction with $d_{\mathrm{Zn}\cdots\mathrm{Zn}}$. As explained in the ‡-footnote in Section 2.1 of the main paper, the correlation interaction is attractive in the sense that it renders Coulomb repulsion of all other electrons with respect to the considered electron i to be minimized by relocating such electrons accordingly, driven by repulsion [2]. For OMOs with lower binding energy E_{bind}, correlation becomes more pronounced as such states are more delocalized and thus can be relocated to a greater extent with the same energy cost as compared to more localized eigenstates. For the i-Zn doped Si NCs, this translates to the top i-Zn OMO being most affected by revoking a bigger portion of the attractive impact of the correlation interaction. Inversely, the bottom i-Zn OMO within the NC energy gap is affected the least by a change in correlation interaction as it is more localized due to its higher E_{bind}. The impact becomes obvious in the right graph of Figure 1 when looking at the asymmetry of the energy splitting which rises proportional to $[d_{\mathrm{Zn}\cdots\mathrm{Zn}}]^{-1}$ as is the case for Pauli blocking. This dependence of correlation interaction on E_{bind} of the considered i-Zn OMOs also explains why the average energy of all i-Zn frontier OMOs in the NC energy gap of the $\mathrm{Si}_{286}\mathrm{H}_{144}$ NC with 2× i-Zn half-way into the NC is slightly *higher* (average E_{bind} is slightly *lower*) as opposed to the same NC with 4× i-Zn half-way into the NC, see right graph in Figure 1.

2 Calculation of the surface plasmon frequency for a ML of i-TM doped Si NCs

For the derivation of the surface plasmon frequency f_{SurfPls}, we follow Yu & Cardona [3, 4], and treat the plasmonic oscillation within the framework of a sum of harmonic oscillators. Using the Kramers-Heisenberg dielectric function in this context [5] and setting the damping coefficient for the harmonic oscillators of metallic solids (resonant electrons) γ to zero[2], we get

$$f_{\mathrm{SurfPls}} = \frac{\omega_{\mathrm{SurfPls}}}{2\pi} \quad = \quad \sqrt{\frac{n\,\epsilon_V\,e^2}{\varepsilon_0\left[\varepsilon_{\mathrm{opt}}(\mathrm{Si\ NC}) + \varepsilon_{\mathrm{opt}}(\mathrm{H_2O})\right] m_0\, m_{\mathrm{eff}}}}\ . \tag{1}$$

Here, n is the density of loosely bound valence electrons at i-TM dopants, ϵ_V is a volume correction factor accounting for the packing density of NCs (see discussion below), e is the elementary charge, $\varepsilon_{\mathrm{opt}}(\mathrm{Si\ NC}) = 3.12$ is the specific dielectric constant of Si NCs (host lattice) treated here[3], $\varepsilon_{\mathrm{opt}}(\mathrm{H_2O})$ is the relative dielectric constant of $\mathrm{H_2O}$ at the calculated value of f_{SurfPls} [7], ε_0 is the dielectric constant of vacuum, m_0 is the electron rest mass, and $m_{\mathrm{eff}} := 1$ is the effective electron mass in the atomic limit (vs. Bloch band picture of a solid). Since $\varepsilon_{\mathrm{opt}}(\mathrm{H_2O})$ is a function of f_{SurfPls}, equation 1 has to be solved by iteration.

The nominal electron density n in the NC volume is twice the density of i-Zn dopants (each Zn atom has two valence electrons in its frontier OMOs in the NC gap). Working with the doping density of 4.65×10^{19} cm^{-3} of the $\mathrm{Si}_{455}\mathrm{H}_{196}$ NC of 26 Å size and with 2× Zn near its surface for maximum radiation efficiency η_{rad}, we arrive at $n = 9.3 \times 10^{19}$ cm^{-3}. We presume that all Si NCs have a spherical shape and are arranged in a hexagonal closed-packing (hcp) geometry as a monolayer (ML), and allow some space Δd between neighbouring NCs. Such a geometry is shown in figure 2. For the NCs in hcp geometry, we have three sphere sectors of $^1/_6\,V_{\mathrm{NC}}$ each within the volume of the primitive cell, whereby V_{NC} is the NC volume, *cf.* Figure 2. From this observation, we can obtain the NC volume within the volume primitive cell as

$$V_{\mathrm{NC}}(\mathrm{UC}) \quad = \quad \frac{1}{2}V_{\mathrm{NC}} \quad = \quad \frac{\pi}{12}d_{\mathrm{NC}}^3\ . \tag{2}$$

The volume of the primitive hcp cell is an equilateral prism of side length $d_{\mathrm{NC}} + \Delta d$

$$V_{\mathrm{prism}}(\mathrm{UC}) \quad = \quad A_{\mathrm{G}}\,h \quad = \quad \frac{\sqrt{3}}{4}\left[d_{\mathrm{NC}} + \Delta d\right]^3, \tag{3}$$

whereby Δd provides a distance between the apexes of adjacent NCs as per discussion below. The ratio of both volumes provides us with the volume correction factor ϵ_V for the hcp geometry:

$$\epsilon_V \quad = \quad \frac{V_{\mathrm{NC}}(\mathrm{UC})}{V_{\mathrm{prism}}(\mathrm{UC})} \quad = \quad \frac{\pi}{3\sqrt{3}}\left[\frac{d_{\mathrm{NC}}}{d_{\mathrm{NC}} + \Delta d}\right]^3\ . \tag{4}$$

---

[2] Setting $\gamma = 0$ results in the imaginary part (extinction or absorbance) to vanish.

[3] Since Si is a covalent solid, we have no change in the dielectric response over excitation energy, *i.e.* $\varepsilon_{\mathrm{opt}} = \varepsilon_{\mathrm{stat}}$[6], see end of Sect. 2.1 in main publication.

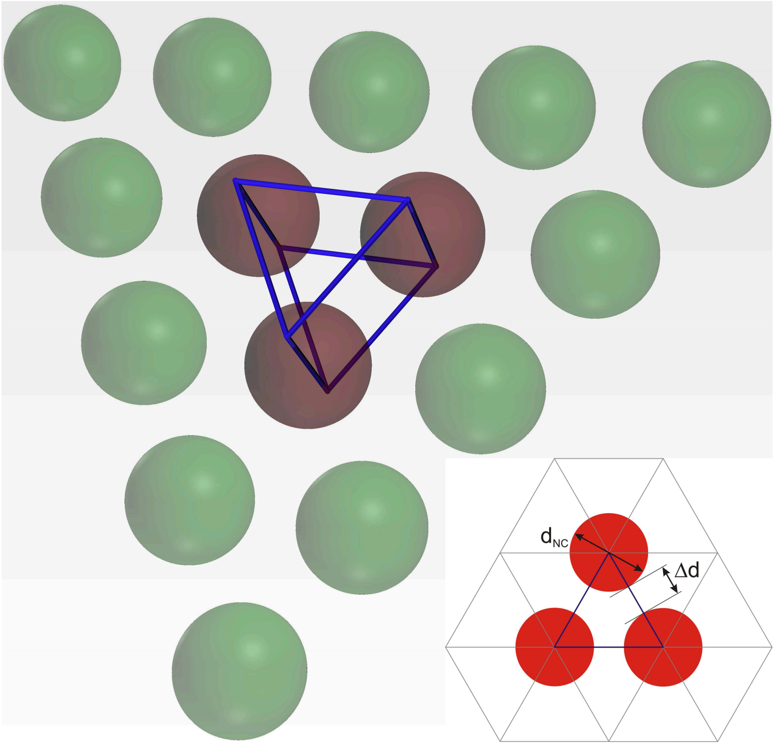

Figure 2: Monolayer (ML) of spherical Si NCs in hexagonal close-packed (hcp) geometry, with the primitive volume cell shown as blue frame and the associated spheres shown in red (big graph). The inset on the right lower corner shows the top view of the primitive volume cell in blue (and its translational/rotational replication) with the three spheres participating in the filling of the primitive volume cell, along with the diameter of the NC d_{NC} and the inter-NC distance Δd which is filled with a matrix material such as an aqueous solution. The primitive volume cell sticks out beyond the NCs by $\frac{1}{2}\Delta d$ in z-direction to cover the matrix covering the top and bottom surface of the hcp NC ML.

We now presume that all Si NCs are ethyl-amino ($-\mathrm{CH_2{-}CH_2{-}NH_2}$) capped [8] which corresponds to a shell thickness of ca. 4 Å [9]. In an aqueous environment, we further assume that there is 2 Å of $\mathrm{H_2O}$ (ca. 1 to 2 ML) between the capped apexes where the Si NCs are closest to each other, adding up to $\Delta d = 10$Å between Si NCs cores in total. Ethyl-amino ligands have a relative dielectric constant in the range of aminoalkyd resin [10] which has $\varepsilon_{\mathrm{opt}} \approx 4$. From iterating for f_{SurfPls}, we get $\varepsilon_{\mathrm{opt}}(\mathrm{H_2O}, f_{\mathrm{SurfPls}}) = 5.3$ for the convergence of equation 1. Hence, we presume that the ethyl-amino shell around the Si NC core has the *same* relative dielectric constant as the $\mathrm{H_2O}$ surrounding the capped NCs, *viz.* $\varepsilon_{\mathrm{opt}}(-\mathrm{CH_2{-}CH_2{-}NH_2}) = \varepsilon_{\mathrm{opt}}(\mathrm{H_2O}, f_{\mathrm{SurfPls}}) = 5.3$. As a consequence, f_{SurfPls} in equation 1 will be underestimated by roughly 10 % (depending on NC size; d_{NC} *vs.* Δd, see equation 4). This underestimation should cancel out with the non-zero damping ($\gamma > 0$) which occurs due to surface plasmons passing on their energy to the Si NC lattice via phonon generation. The generated phonons increase the average thermal energy of the Si atoms $k_{\mathrm{B}}T$, thereby their temperature and consequentially the temperature of their immediate environment as well.

Follwing above discussion, we obtain $\epsilon_V = 0.220$ for the $\mathrm{Si_{455}}$ NC core of 26 Å size, and eventually can iterate equation 1 for a self-consistent $\varepsilon_{\mathrm{opt}}(\mathrm{H_2O}, f_{\mathrm{SurfPls}}) = 5.30$ to arrive at $f_{\mathrm{SurfPls}} \approx 140$ GHz for doping with 2× i-Zn. For the same Si NC doped with 2× i-Cu at the same position, we arrive at $f_{\mathrm{SurfPls}} \approx 96$ GHz due to a slight increase in $\varepsilon_{\mathrm{opt}}(\mathrm{H_2O}, f_{\mathrm{SurfPls}})$ and the nominal electron density due to the loosely bound valence electrons of the two i-Cu atoms being two instead of four. For the $\mathrm{Si_{286}H_{144}}$ NC of 22 Å size with $\Delta d = 10$ Å, we obtain $\epsilon_V = 0.198$ and $f_{\mathrm{SurfPls}}(\varepsilon_{\mathrm{opt}}[\mathrm{H_2O}] = 5.75) \approx 195$ GHz for doping with 2× i-Sc (three valence electrons each, $n = 8.29 \times 10^{19}$ $\mathrm{cm^{-3}}$). For the bigger $\mathrm{Si_{455}H_{196}}$ NC of 26 Å size and $\Delta d = 10$ Å, we use $\epsilon_V = 0.220$ from above and arrive at $f_{\mathrm{SurfPls}}(\varepsilon_{\mathrm{opt}}[\mathrm{H_2O}] = 5.30) \approx 120$ GHz for doping with 2× i-Sc ($n = 1.4 \times 10^{20}$ $\mathrm{cm^{-3}}$). We note here that Sc possesses three valence electrons (vs. two for Zn and one for Cu). The smaller of the above i-Sc doped Si NCs is subject to further discussions in the following section.

3 Data on Si nanocrystals containing other 4s3d transition metal interstitial dopants: Sc as an example

The 4s3d TMs have the trend of increasing atomic radii with a decreasing number of valence (4s and 3d) electrons [9]. For Zn and Cu, the respective atomic radius is $r_{\mathrm{Zn}}^{\mathrm{atom}} = 1.335$ Å and $r_{\mathrm{Zn}}^{\mathrm{atom}} = 1.278$ Å. The opposite end of the 4s3d TM period is represented by Sc which has $r_{\mathrm{Sc}}^{\mathrm{atom}} = 1.606$ Å. The structural optimization of Si NCs with i-Zn and i-Cu dopants in the framework of Hartree-Fock (HF) theory [2, 11–13], featuring exact exchange interaction, converged without compromising the integrity of the Si NC lattice; i-TM dopants settled on assigned interstitial locations as a function of their quantum-chemical atomic properties. The question raises whether bigger TM metal atoms (as per $r_{\mathrm{TM}}^{\mathrm{atom}}$) can still be fitted into interstitial positions within the Si NC host lattice without distorting or even disintegrating the NC or alternatively undergoing out-diffusion, a phenomenon which is known as self-purification [14–16]. Here, Sc can serve as a benchmark to verify to what extent and from what NC size downwards such processes occur. We have demonstrated by DFT that i-Cu [8] and i-Zn (see main publication) in $\mathrm{Si}_{84}\mathrm{H}_{64}$ NCs as small as $d_{\mathrm{NC}} = 15$ Å can be accommodated. In accord with these findings, no issues were encountered when including up to six i-Cu dopants into ethyl-amino capped Si NCs with $d_{\mathrm{NC}} \geq 25$ Å in experiment [8].

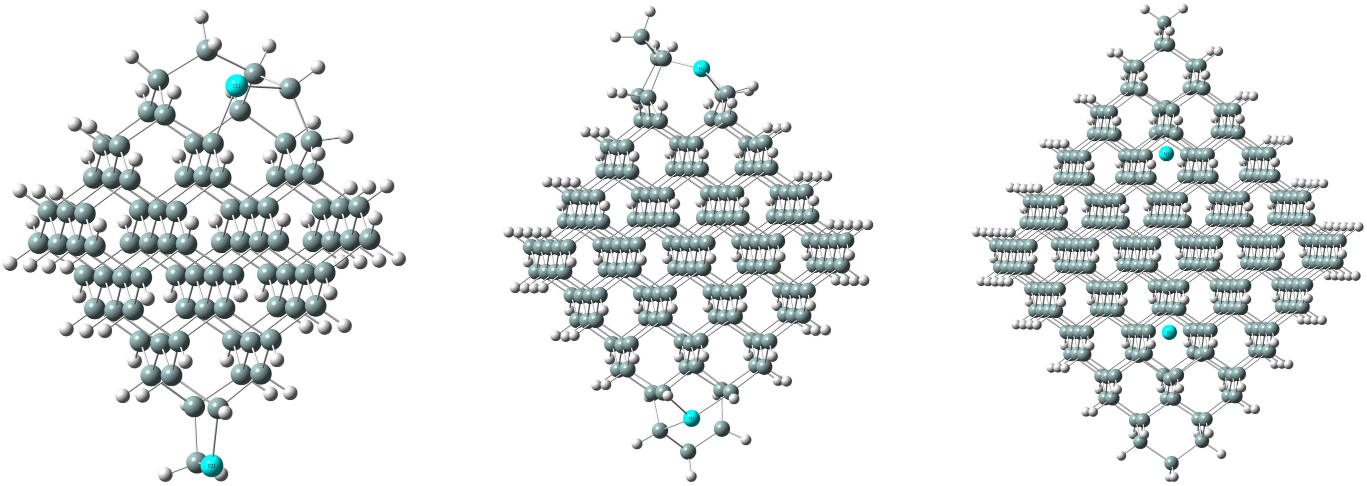

Figure 3: $\mathrm{Si}_{84}\mathrm{H}_{64}$ ($d_{\mathrm{NC}} = 15$ Å, with 2× i-Sc originally near its surface; left), $\mathrm{Si}_{165}\mathrm{H}_{100}$ ($d_{\mathrm{NC}} = 18.5$ Å, with 2× i-Sc originally near its surface; centre), and $\mathrm{Si}_{286}\mathrm{H}_{144}$ ($d_{\mathrm{NC}} = 22.2$ Å, with 2× i-Sc half-way into NC; right) approximants after structural optimization. Atom colours: Si is grey, H is white, and i-Sc is cyan. All approximants are shown along $\langle 110 \rangle$ direction. Disintegration and re-bonding around the Sc atoms is evident, leading to metastable Sc^{2+} for the $\mathrm{Si}_{84}\mathrm{H}_{64}$ NC and to stable Sc^{3+} plus two Si dangling bonds for the $\mathrm{Si}_{165}\mathrm{H}_{100}$ NC. At the bigger $\mathrm{Si}_{286}\mathrm{H}_{144}$ approximant, we can see a notable distortion of the local Si lattice around both i-Sc dopants. Ionization numbers on Sc refer to oxidation numbers and do not reflect their actual positive charge.

With shrinking NC size, less bonds and atoms of the Si NC lattice [16] have to compensate the stress which is exerted by an i-TM dopant, until a minimum size limit $d_{\mathrm{NC}}^{\mathrm{min}}$ is reached below which the NC gets structurally compromised, or the i-TM dopant diffuses out of the NC. For the $\mathrm{Si}_{84}\mathrm{H}_{64}$ NC with 15 Å size, there are 1.62 internal bonds per Si atom, rising to 1.70 internal bonds per Si atom for the $\mathrm{Si}_{165}\mathrm{H}_{100}$ NC with 18.5 Å size[4] to cope with stress exerted on the NC lattice [16]. For i-Sc, this $d_{\mathrm{NC}}^{\mathrm{min}}$ appears to be the just reached with the $\mathrm{Si}_{286}\mathrm{H}_{144}$ NC with $d_{\mathrm{NC}} = 22.2$ Å and a corresponding 1.75 internal bonds per Si atom, and only if i-Sc dopants are placed deeper (half-way) into the NC[5], *cf.* Figure 3 (right). Stress compensation in this approximant still leads to notable distortions in the local Si lattice around the i-Sc dopants. For $d_{\mathrm{NC}} < 22.2$ Å, Si NCs get severely compromised by Si—Si bond breakage, generation of Si dangling bonds (DBs) in the process, and Sc forming bonds with peripheral Si atoms, possibly even in a metastable state as occurring in the $\mathrm{Si}_{84}\mathrm{H}_{64}$ NC featuring di-valent Sc, see Figure 3 (left).

Since all other 4s3d TMs have a lower $r_{\mathrm{TM}}^{\mathrm{atom}}$ as compared to Sc, it is save to say that for $d_{\mathrm{NC}} \geq 22.2$ Å, the Si NCs preserve their lattice structure and bond geometry, though minor local lattice distortions may occur. Regarding

---

[4] Asymptotic limit for bulk Si is 2 bonds per Si atom (four bonds per Si atom, each bond shared between two atoms), see [16].

[5] Placing 2× i-Sc into the $\mathrm{Si}_{286}\mathrm{H}_{144}$ NC near its surface results in out-diffusion of such Sc atoms (self-purification effect).

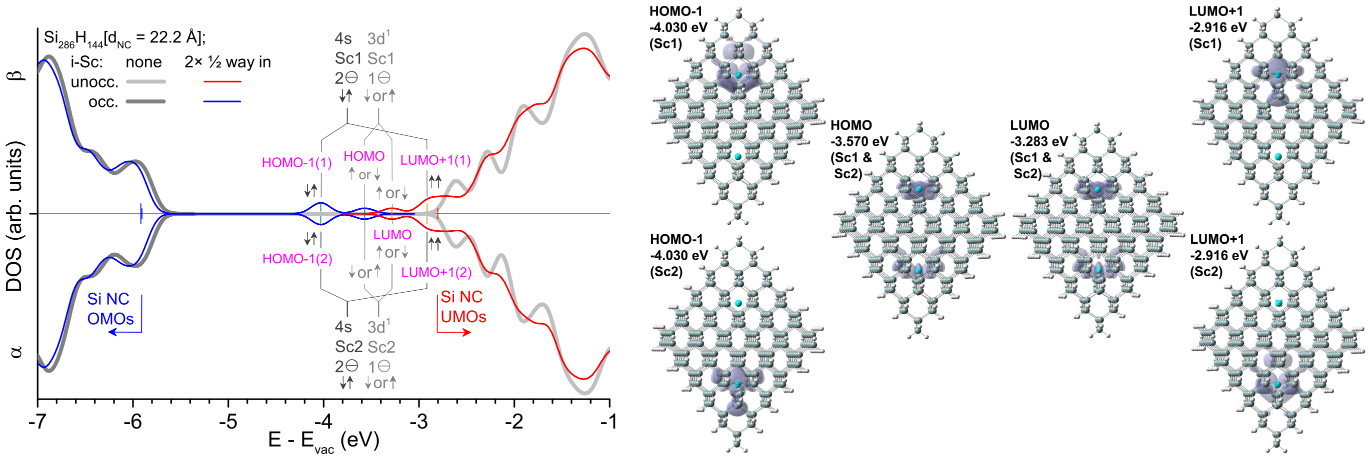

Figure 4: Electronic DOS of the $Si_{286}H_{144}$ approximant ($d_{\mathrm{NC}} = 22.2$ Å) with 2× Sc located half-way into the NC (left graph), *cf.* Figure 3, right graph. Listed details of frontier MOs associated with Sc show occupancy, location and bonding-antibonding splitting of respective MOs in accord with crystal field theory [9, 17, 18], see text. The approximant has a singlet configuration in its ground state, meaning that MOs are either fully occupied with two electrons or fully unoccupied (no electrons). Please observe that HOMO−1 and HOMO+1 are each doubly degenerate; they exist as two MOs with the same eigenenergy, one at the Sc 1 and the other at the Sc 2 atom. Respective MO distributions (graphs on right) are shown as iso-plots of their density – $\langle\psi|\psi'\rangle$ – in the same sequence as occurring in the DOS graph. The iso-surface of particle densities is 4×10^{-4} $e/a_{\mathrm{B},0}$ (6.8×10^{-3} $e/\text{Å}^3$) throughout.

5s4d-TMs, we find that, apart from Y, all other TMs of this period would fit on i-sites in Si NCs, though their increased toxicity may render any efforts for cell marking as counterproductive [9]. Relativistic orbit contraction of core electrons in 6s5d-TMs results in their $r_{\mathrm{TM}}^{\mathrm{atom}}$ values to shrink, allowing even La to be used as an i-TM dopant from a structural point of view. Regarding biocompatibility, a possible cohort of 5s4d- and 6s5d-TM candidates is given by the metals of the Pt group and adjacent TMs, that is, Ru, Rh, Pd, Ag, and Re, Ir, Pt and Au. Self-purification by out-diffusion of the TM atoms requires much less energy and therefore is considerably more difficult to assess in terms of probability to occur, being complicated further by its dependence on the diffusion coefficient as a function of temperature (processing conditions) and type of TM. However, these considerations imply that – unlike Cu and Zn [19] – Sc and other TMs with similar $r_{\mathrm{TM}}^{\mathrm{atom}}$ such as Ti are unlikely to get located on i-sites within Si NCs with $d_{\mathrm{NC}} \leq 25$ Å at or near room temperature. While excitation with UV photons surely facilitates photochemical reactions such as bond modifications at Si NC interfaces [20], dopant diffusion is driven by the thermal energy $k_{\mathrm{B}}T$ in compound with a significant momentum, requiring appropriate kinetic mass. Since photons have a momentum (kinetic mass) of virtually nil, they cannot promote dopant diffusion. On the other hand, a Si lattice at high temperatures can provide considerable momentum to the dopant via phonon transfer [21] until the thermal (kinetic) energy of the dopant is in equilibrium with the Si lattice, enabling dopant diffusion via Fick's law [22].

The optical transition we consider for i-Sc in terms of spectroscopical applications on human tissue are those from its frontier OMOs within the energy gap to the frontier OMOs of the nominal Si NC. Such transitions in the visible spectrum play a major role in the photoluminescence (PL) of such doped NCs, see to our recent work on i-Cu [8]. These MOs become unoccupied under excitation, allowing for radiative emissions from the HOMO−1 and HOMO state associated with Sc to the frontier OMOs associated with the nominal NC, having an energy of ca. 1.88 eV and 2.34 eV ($\lambda_{\mathrm{PL}} \approx 660$ nm and 530 nm), respectively. The more complex MO structure of Sc as compared to Cu results in stronger MO energy splitting, yielding to four states within the nominal NC energy gap. The dispersion of optical transitions to different energies and radiative efficiencies η_{Rad} counteracts the goal of an intense narrow-band emission. These findings again emphasize the excellent properties of i-Zn as Si NC dopant where the nearly exact midgap position of its frontier OMOs allows for a nearly monochromatic emission, originating from *both*, the LUMO-HOMO transitions, and the transition from frontier OMOs associated with i-Zn to frontier OMOs of the nominal NC, see near the end of Section 2.1 in main publication. In contrast to Zn where the completely filled 3d shell is too stable to provide electronic states within the NC energy gap, the $3d^1$ atomic orbital (AO) of Sc does interfere with its 4s AOs, achieving significant MO level splitting due to missing 3d-4s hybridization.

The fundamental optical transitions, namely between frontier OMOs and UMOs of the two i-Sc dopants, result in comparatively low transition energies. Notwithstanding, such transitions are instrumental in understanding the nature of i-Sc as an optical centre in Si NCs. There are three groups of transitions (for six-digit energy values, see to discussion about eigenenergies below). Group 1 features HOMO $\rightleftharpoons$ LUMO+1 (Sc 1 $\rightleftharpoons$ Sc 2) and HOMO $\rightleftharpoons$ LUMO+1 (Sc 2 $\rightleftharpoons$ Sc 1) with transition energies $E_{\mathrm{tr}} = 0.169807$ and 0.169838 eV, respectively, and $f_{\mathrm{osc}} = 2 \times 10^{-4}$ each; group 2 featuring HOMO−1 $\rightleftharpoons$ LUMO (Sc 1 $\rightleftharpoons$ Sc 2) and HOMO−1 $\rightleftharpoons$ LUMO (Sc 2 $\rightleftharpoons$ Sc 1) with transition energies $E_{\mathrm{tr}} = 0.250548$ and 0.250436 eV, respectively, and $f_{\mathrm{osc}} = 5 \times 10^{-4}$ each; group 3 consisting of of four transitions, where HOMO−1 $\rightleftharpoons$ LUMO+1 (Sc 1 $\rightleftharpoons$ Sc 1) and HOMO−1 $\rightleftharpoons$ LUMO+1 (Sc 2 $\rightleftharpoons$ Sc 2) dominate the optical transition by far with $E_{\mathrm{tr}} = 0.367$ eV and a total $f_{\mathrm{osc}} = 0.153$. The latter value exceeds the optical activity of the two other transition groups by a factor of ca. 380 and 150, respectively. We derive from above data that the dominant PL would occur at $\lambda_{\mathrm{PL}} \approx 3.38\ \mu$m.

When subtracting the excited ground state (GS) energy (the quasi-particle transition) from the initial GS energy, we obtain the exciton binding energy $E_{\mathrm{exc}}^{\mathrm{bind}}$[6]. The Hamiltonian for the exciton binding energy is $\mathcal{H}_{\mathrm{exc}} \propto [a_{\oplus-\ominus}]^{-1}$, with $a_{\oplus-\ominus}$ as the exciton radius (distance between electron and hole coordinates within NC). In $\mathcal{H}_{\mathrm{exc}}$, we omitted identical parameters (e^2, ε_0 and $\varepsilon_{\mathrm{NC}}$) which are given as a constant either by nature or by the NC considered here. We immediately see from the bare form of $\mathcal{H}_{\mathrm{exc}}$ that the most localized excitons will have the highest value of $E_{\mathrm{exc}}^{\mathrm{bind}}$. For the three transition groups, we obtain $E_{\mathrm{exc}}^{\mathrm{bind}}$(group 1) = 0.484 eV, $E_{\mathrm{exc}}^{\mathrm{bind}}$(group 2) = 0.497 eV, and $E_{\mathrm{exc}}^{\mathrm{bind}}$(group 3) = 0.748 eV. We see from those values that the group 3 transitions must be significantly more localized as compared to the group 1 and 2 transition groups. The reason for this deviation becomes apparent when looking at the occupation diagram in the electronic DOS of the $\mathrm{Si}_{286}\mathrm{H}_{144}$ approximant, *cf.* Figure 4, left graph. The dominant transitions of group 3 start *and* end in 4s↑↓-dominated states which are more localized at their respective Sc atom and do not readily hybridize with other states as explained below. The high optical activity of such states expressed by f_{osc} likely originates from a high overlap integral of initial and final states $\langle\psi_{\mathrm{MO}}^{\mathrm{ini}}|\psi_{\mathrm{MO}}^{\mathrm{fin}}\rangle$ because both are located at the same atom.

Looking at the eigenenergies of both fully occupied 4s-based HOMO−1 states (4s ↑↓ each), one located at the Sc 1, the other located at the Sc 2 atom, *cf.* Figure 4, we note a minute energy difference of $\Delta E = 31\ \mu$eV. We also note that there is an even smaller difference in energy of $\Delta E = 8\ \mu$eV between LUMO+1(Sc 1) and LUMO+1(Sc 2). Obviously, such ΔE values have no practical consequences as $k_{\mathrm{B}}T$ exceeds them by three orders of magnitude. What these tiny ΔE values show is that the local environment – the Si host lattice – has a slightly different impact as per i-Sc dopant. For the HOMO+1 states, ΔE is smaller as these states are less localized and hence can evade the change in local environment to a higher degree. Apart from a slight variation in individual Si atomic charges, slightly different atomic positions of the Si host lattice around Sc atoms due to a stress response to the i-Sc atoms can be the cause, *cf.* Figure 3, right graph. The HOMO−1 and consequently LUMO+1 states do not undergo hybridization between the two i-Sc atoms since the full 4s shell is comparatively inert, the mentioned MOs are reasonably localized around their Sc atom, and the distance between Sc atoms being $d_{\mathrm{Sc}\cdots\mathrm{Sc}} = 11.23$ Å is about the 4-fold value of the bond length of co-valent Sc [9]. To add, crystal field theory [9, 17, 18] predicts that 4s-3d hybridization does not occur. Rather, 4s electrons may be re-located to 3d states and *vice versa*, promoted by an increase in E_{bind} for the entire 4s3d electron ensemble. The situation for the HOMO and LUMO which are defined by $3\mathrm{d}^1$ and $3\mathrm{d}^{1*}$ states is different. These MOs are less localized (lower E_{bind}), and can hybridize with their counterpart at the other Sc atom since the $3\mathrm{d}^1$ states are only half-occupied and therefore can gain E_{bind} by hybridization.

References

[1] W. Pauli, *Zeitschr. Phys.*, 1925, **31**, 765–783.

[2] R. M. Martin, *Electronic Structure – Basic Theory and Practical Methods*, Cambridge University Press, Cambridge, 2004.

[3] P. Y. Yu and M. Cardona, *Fundamentals of Semiconductors – Physics and Materials Properties*, Springer, Berlin, 4th edn, 2010.

---

[6] We point out here that the quasi-particle excitation energy presents the vertical transition (direct, no electron-phonon interaction) which includes $E_{\mathrm{exc}}^{\mathrm{bind}}$ but no lattice relaxation (electron-phonon interaction). Since the Si NCs are very small (discrete phononic DOS and quasi-direct fundamental electronic gap) and located in an aqueous solution (hence experience high electrodynamic screening), the quasi-particle approximation yields a good estimate for $E_{\mathrm{exc}}^{\mathrm{bind}}$.

[4] M. Cardona, *Am. J. Phys.*, 1971, **39**, 1277.

[5] H. Kuzmany, *Solid-State Spectroscopy – An Introduction*, Springer, Berlin, 1998.

[6] K. W. Böer, *Survey of Semiconductor Physics, Vol. 1*, Van Nostrand Reinhold, New York, 1990.

[7] W. J. Ellison, K. Lamkaouchi and J.-M. Moreau, *J. Molec. Liq.*, 1996, **68**, 171–279.

[8] B. F. P. McVey, D. König, X. Cheng, P. B. O'Mara, P. Seal, X. Tan, H. A. Tahini, S. C. Smith, J. J. Gooding and R. D. Tilley, *RSC Nanoscale*, 2018, **10**, 15600–15607.

[9] A. F. Holleman, E. Wiberg and N. Wiberg, *Lehrbuch der Anorganischen Chemie (101. Ed.)*, Walter deGruyter, Berlin, 95th edn, 1995.

[10] Clipper Controls Inc., CA , `http://www.clippercontrols.com/pages/Dielectric-Constant-Values.html#A`, assessed on September 11, 2020.

[11] D. R. Hartree, *Proc. Cambr. Phil. Soc*, 1928, **24**, 89–110.

[12] D. R. Hartree, *Proc. Cambr. Phil. Soc*, 1928, **24**, 111–132.

[13] V. Fock, *Zeitschr. Phys.*, 1930, **61**, 126–148.

[14] G. M. Dalpian and J. R. Chelikowsky, *Phys. Rev. Lett.*, 2006, **96**, 226802.

[15] A. R. Stegner, R. N. Pereira, R. Lechner, K. Klein, H. Wiggers, M. Stutzmann and M. S. Brandt, *Phys. Rev. B*, 2009, **80**, 165326.

[16] D. König, *AIP Adv.*, 2016, **6**, 085306.

[17] H. A. Bethe, *Ann. Phys.*, 1929, **3**, 133–208.

[18] J. H. Van Vleck, *Phys. Rev.*, 1932, **41**, 208–215.

[19] B. McVey, J. Butkus, J. E. Halpert, J. M. Hodgkiss and R. D. Tilley, *Phys. Chem. Lett.*, 2015, **6**, 1573–1576.

[20] M. Dasog, Z. Yang, S. Regli, T. M. Atkins, A. Faramus, M. P. Singh, E. Muthuswamy, S. M. Kauzlarich, R. D. Tilley and J. G. C. Veinot, *ACS Nano*, 2013, **7**, 2676–2685.

[21] D. König, Y. Yao, B. Puthen-Veettil and S. C. Smith, *Semicond. Sci. Technol*, 2020, **35**, 073002.

[22] K. W. Böer, *Survey of Semiconductor Physics, Vol. 2*, Van Nostrand Reinhold, New York, 1992.